Quaternary Research (2018), **89**, 629–644.

doi:10.1017/qua.2017.83

SPECIAL ISSUE
INQUA LoessFest 2016

Magnetostratigraphic dating of the Linyi Fauna and implications for sequencing the mammalian faunas on the Chinese Loess Plateau

Yahui Qiu[a,b], Hong Ao[b,c]*, Yunxiang Zhang[a]*, Peixian Shu[b,d], Yongxiang Li[a], Xingwen Li[b], Peng Zhang[b]

[a]State Key Laboratory of Continental Dynamics, Department of Geology, Northwest University, Xi'an 710069, China
[b]State Key Laboratory of Loess and Quaternary Geology, Institute of Earth Environment, Chinese Academy of Sciences, Xi'an 710061, China
[c]Lamont-Doherty Earth Observatory, Columbia University, Palisades, New York 10964, USA
[d]College of Earth Sciences, University of Chinese Academy of Sciences, Beijing 100049, China

(Received April 20, 2017; Accepted August 17, 2017)

Abstract

The Chinese Loess Plateau (CLP) in North China is an important terrestrial archive that witnessed the environmental changes and mammal and early human evolution in Asia over the past 2.6 Ma. Establishing precise ages for the Pleistocene faunas on the CLP is critical for better understanding of these environmental, biological, and archaeological issues. Here we report a new magnetostratigraphic record that places age constraints on the Linyi Fauna on the southeastern CLP. Our investigated 170-m-thick Linyi section mainly consists of two portions: (1) an overlying eolian Quaternary loess-paleosol sequence and (2) underlying fluvial-lacustrine sand and silty clay. Paleomagnetic results suggest that the composite section records the Brunhes chron, Jaramillo and Olduvai subchrons, and successive reverse polarity portions of the intervening Matuyama chron. The Linyi Fauna is located between Jaramillo and Olduvai subchrons in the fluvial-lacustrine interval, with an estimated age of ~1.5–1.6 Ma. Combining previously dated faunas, we establish a Pleistocene magnetochronology spanning from 2.54 to 0.65 Ma for the faunas on the CLP.

Keywords: Magnetochronology; Chinese Loess Plateau; Pleistocene; Mammalian fauna; Paleoenvironment

INTRODUCTION

The Chinese Loess Plateau (CLP) is situated near the middle reaches of the Yellow River, North China, extending from ~100°E to 115°E and from ~34°N to 41°N (Fig. 1). It hosts a vast expanse of thick and continuous Quaternary terrestrial sediments that not only record past environment changes, but also are rich in Paleolithic archaeological materials and faunal sites (Liu, 1985; Wen, 1989; An et al., 1991; Ding et al., 1995; Porter and An, 1995; Xiao et al., 1995). Mammals are sensitive to environmental changes and were important food resources for early humans. Thus, they have important implications for environmental and early human evolution.

Starting from the early 1920s, a large number of faunal sites have been found on the CLP (Tong et al., 2008) (Fig. 1 and Tables 1 and 2). The Linyi Fauna is an important Early Pleistocene fauna that was found in the Yuncheng Basin, southeastern CLP, in 1959 and has yielded abundant mammalian fossils (Zhou and Zhou, 1959, 1965; Tang et al., 1983). Although mammalian components suggest a broad age range within the Early Pleistocene (Zhou and Zhou, 1959, 1965; Tang et al., 1983), its precise numerical age remains unknown. Here, we present a new paleomagnetic study that constrains the age of the Linyi Fauna. Combining previously dated Pleistocene faunas, we can establish the chronological sequencing of the mammalian faunas on the CLP.

REGIONAL SETTING

At present, the Yuncheng Basin has a mean annual precipitation of 510 mm and a mean annual temperature of 13.5°C. Our studied Linyi section (35°07′29.5″N, 110°23′45.3″E) is located on the eastern bank of the Yellow River. It has a stratigraphic thickness of 170 m and consists of two parts: an overlying eolian Quaternary yellowish loess-paleosol sequence that consists of 15 layers of paleosol and 14 layers of loess (82 m) with underlying fluvial-lacustrine silty clay and sand (the so-called Sanmen Formation, ~88 m thick) that

*Corresponding authors at: State Key Laboratory of Loess and Quaternary Geology, Institute of Earth Environment, Chinese Academy of Sciences, Xi'an 710061, China (H. Ao); State Key Laboratory of Continental Dynamics, Department of Geology, Northwest University, Xi'an 710069, China (Y. Zhang). E-mail addresses: aohong@ieecas.cn (H. Ao); yxzhang@nwu.edu.cn (Y. Zhang).

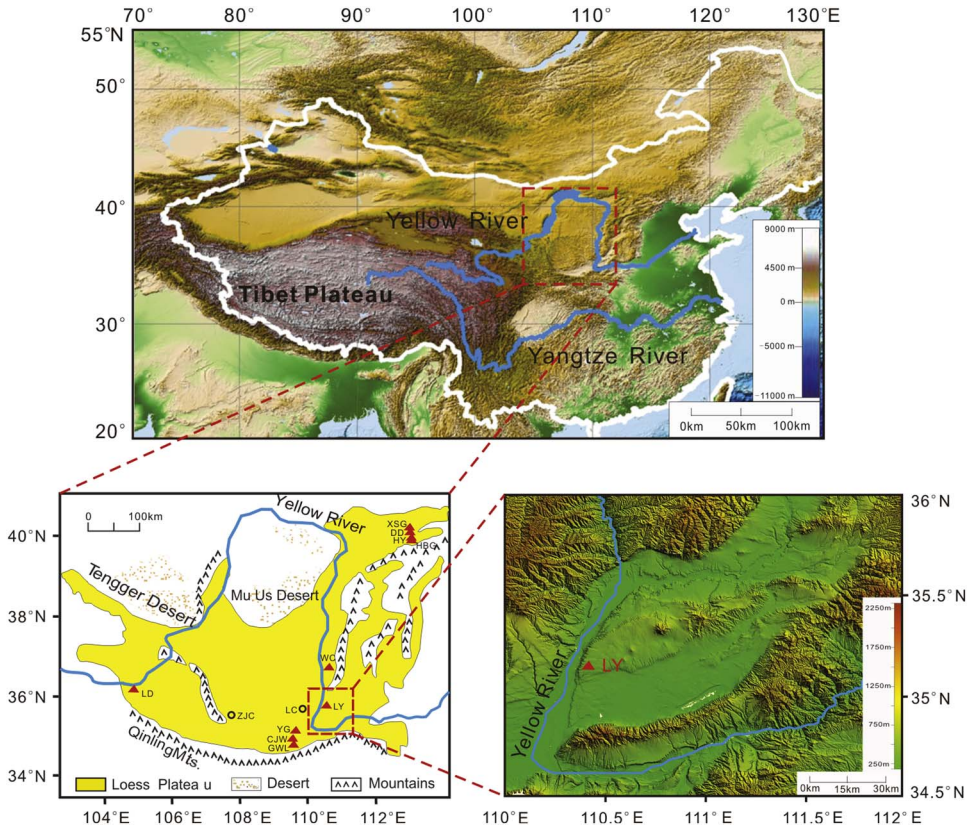

Figure 1. Map with Asian topography (modified from Li et al., 2017), Chinese Loess Plateau (CLP; modified from Ao et al., 2016), Linyi section, and other faunal or section sites mentioned in the text. The red triangles and squares represent the faunal or section sites. CJW, Chenjiawo; DD, Daodi; GWL, Gongwangling; HBG, Huabaogou; HY, Hongya; LC, Luochuan; LD, Longdan; LY, Linyi; WC, Wucheng; XSG, Xiashagou; YG, Yangguo; ZJC, Zhaojiachuan. (For interpretation of the references to color in this figure legend, the reader is referred to the web version of this article.)

consists of 14 sand and silty clay packages. The Linyi Fauna occurs in a sand layer at a depth of 124–127 m below the top of the section (Fig. 2). The Linyi Fauna contains more than 30 mammal species, many of which are similar to other Early Pleistocene faunas in North China (Zhou and Zhou, 1959, 1965; Tang et al., 1983). For example, the presence of *Equus sanmeniensis*, *Hipparion* sp., *Proboscidipparion sirense*, *Cazella* sp., and *Ursus* sp. (Tables 1 and 2) makes it comparable with the nearby Wucheng Fauna (1.2–1.9 Ma) (Yue et al., 1994, 1998; Yue and Xue, 1996). The presence of *Equus sanmeniensis*, *Proboscidipparion sirense*, *Axis shansius*, and *Axis rugosus* makes it comparable with the Yangguo Fauna (0.9–1.0 Ma) (Yue et al., 1994). The Wucheng and Yangguo locations are ~200 km north and southwest of the Yuncheng Basin, respectively.

SAMPLING AND METHODS

To obtain samples that were as fresh as possible, weathered surfaces were removed from the outcrop (at least the surface-most 20 cm). From the entire Linyi section, 98 oriented block samples were taken at 50–100 cm intervals from the

Table 1. List of the Linyi mammalian fauna (from Zhou and Zhou, 1959, 1965; Tang et al., 1983).

Axis shansius	*Axis rugosus*	*Archidiskodon* cf. *planifrons*
Bison sp.	*Canis* sp.	*Cyprinidae* indet.
Coelodonta antiquitatis	*Cazella* sp.	*Cervus* sp.
Emydide indet.	*Equus sanmeniensis*	*Eucteroceros* sp.
Hipparion sp.	*Hyaena* sp.	*Megantereon* sp.
Myospalax fontanieri Milne-Edwards	*Nestoritherium* sp.	*Paracamelus* sp.
Proboscidipparion sirense	*Palaeoloxodon tokunagai* Matsumoto, 1924	*Rusa elegans*
Stegodon cf. zdanskyi Hopwood, 1935	*Sus* sp.	*Tironyx* sp.
Trogontherium sp.	*Ursus* sp.	

Table 2. List of mammalian fauna directly dated by magnetostratigraphy on the Chinese Loess Plateau (Zhou and Zhou, 1959, 1965; Huang and Tang, 1974; Wang, 1982; Tang et al., 1983; Cai, 1987; Zhou et al., 1991; Qiu and Qiu, 1995; Yue and Xue, 1996; Zhang et al., 2003; Cai et al., 2004; Wang et al., 2005; Xue et al., 2006; Li et al., 2008; Liu et al., 2012). (For locations see Figure 1).

	Faunas															
Taxa	LD	WC	GWL	YG	CJW	XSG	DD1	DD2	DD3	DD4	DD5	DD6	DD7	HY	HBG2	HBG1
Aepyosciurus oreintalis	+															
Allicricetus ehiki		+														
Allosiphnus arvicolinus		+														
Apodemus sp.			+					+	+							
Apodemus zhangwagouensis							+	+			+					
Arvicola terrae-rubrae			+													
Ailuropoda melanoleuca fovealis			+													
Axis cf. *rogosus*				+												
A. cf. *shansius*				+												
Axis shansius										+						
Apodemus cf. *sylvaticus*					+											
Apodemus cf. *A. agrarius*								+								
Apodemus cf. *A. atavus*											+					
Alactaga cf. *annulatus*						+										
Antilospira robusta						+										
Acinonyx pleistoceneus						+										
Allocricetus bursae													+			
Antilospira sp.										+						
Antilospiroides hobeiensis																+
Bahomys	+															
Bovinae		+														
Bison palaeosinensis		+				+										
Bahomys hyposodonta			+		+											
Bison				+												
Borsodia chinensis						+										
?*Budorcas* sp.						+										
Canis teilhardi	+															
Canis sp.															+	
Canis multicuspus															+	
C. longdanensis	+															
C. brevicephalus	+															
Chasmaporthetes progressus	+															
Crocuta honanensis	+					+										
Coelodonta nihowanensis	+															
Castor anderssoni	+										+					
Canis chihliensis		+				+										
cf. *Euctenoceros*		+														
Cricetulus cf. *griscus*			+													

Table 2. (*Continued*)

Taxa	Faunas															
	LD	WC	GWL	YG	CJW	XSG	DD1	DD2	DD3	DD4	DD5	DD6	DD7	HY	HBG2	HBG1
C. sp.			+													
Canis variabilis			+													
Capricornis sumatraensis qinlingensis			+													
Cricetulus varians				+												
C. cf. *friseus*				+												
Chasmaporthetes cf. *ossifagus*						+										
Coelodonta sp.						+										
Cervulus bohlini						+										
Cervus elegans						+										
Cervus sp.										+						
Chardina truncatus							+									
Chardinomys nihowanicus							+	+		+	+		+			
Chardinomys yusheensis							+	+	+							
Chilotherium sp.										+				+		
Dicerorhinus lantianensis			+													
D. cf. *mercki*			+													
Dicerorhinus yunchuensis						+										
Dipus fraudator											+					
Eirictis robusta	+															
Equus eisenmannae	+															
Eospalax fontanieri		+														
Equus sanmeniensis		+	+	+		+										
Elaphodus cephalaphus			+													
Elaphurus chinanensis				+												
Elephas					+											
Erinaceus cf. *dealbatus*						+										
Elasmotherium sp.						+										
Equus teilhardi						+										
Elaphurus bifurcatus						+										
Eucladoceros boulei						+										
Felis teilhardi	+															
Felis cf. *palaeosinensis*				+												
Gazella cf. *blacki*	+														+	+
Gazella sp.		+													+	+
Gerbillus sp.			+													
Gazella sinensis				+		+										
G. subgutturosa						+										
Germanomys cf. *G. weileri*									+							
Germanomys sp.								+	+							

Table 2. (*Continued*)

Taxa	Faunas															
	LD	WC	GWL	YG	CJW	XSG	DD1	DD2	DD3	DD4	DD5	DD6	DD7	HY	HBG2	HBG1
Hipparion sp.														+	+	
Hipparion houfenense																+
Hipparion cf. *hippidiodus*															+	
Hipparion (*Proboscidipparion*) *sinensis*	+	+		+												
Hesperotherium sp.	+															
Hemibos gracilis	+															
Homotherium crenatidens	+															
Hypolagus brachypus		+														
Homo erectus			+		+											
Hystrix cf. *subcristata*			+													
Hyaena sinensis			+													
Hystrix subcristata				+												
Hyaena licenti				+												
Hystrix					+											
Hystrix sp.						+										
Homotherium cf. *crenatiders*						+										
Huaxiamys downsi							+									
Huaxiamys primitivus							+									
?*Huaxiamys* sp.							+									
Karnimata sp.										+	+					
Kowalskia similis							+									
Kowalskia sp.							+									
Lynx shansius	+	+		+												
Leptobos brevicornis	+	+	+	+												
L. sp.			+													
L. laochihensis				+												
L. amplifrontalis				+												
Lepus wongi					+											
Lutra licenti						+										
Lynx sp.						+										
Lunanosorex cf. *L. lii*											+					
Leporidae gen. et sp. indet.															+	
Megantereon nihowanensis	+					+										
Marmota parva	+															
Mimomys cf. *gansunicus*	+															
Macaca cf. *anderssoni*	+															
Meles teilhardi	+															
Myospalax chaoyatseni		+		+												
Microtus epiratticeps			+													

Table 2. (*Continued*)

Taxa	Faunas															
	LD	WC	GWL	YG	CJW	XSG	DD1	DD2	DD3	DD4	DD5	DD6	DD7	HY	HBG2	HBG1
Myospalax tingi			+	+	+											
M. fontanieri			+													
M. sp.			+													
Meles cf. *leucurus*			+													
Megantherion lantianensis			+													
Megatapirus augustus			+													
M. arvicolinus				+												
M. cf. *fontanieri*					+											
Mustela pachygnatha						+										
Meles chiai						+										
Mesosiphneus praetingi										+	+					
Micromys tedfordi							+	+	+	+						
Mimomys orientalis									+	+	+					
Mimomys sp.								+	+	+	+					
Mimomys sp. 2										+						
Mimomys stenlini								+								
Nipponicervus longdanensis	+															
Nyctereutes sinensis		+				+									+	
Nestoritherium sinensis			+													
Nannocricetus mongolicus							+	+	+	+	+		+			
Nestoritherium sp.						+										
O. dauurica		+														
Ochotonoides complicidens			+													
Ochotona cf. *thibetana*			+													
Ochotonoides complicidens					+	+										
Ovis shantungensis						+										
Ochotona minor											+					
Ochotona sp.								+	+			+				
Paradolichopithecus gansuensis	+															
Pachycrocuta licenti	+															
Panthera palaeo sinensis	+															
Proboscidipparion sinensis		+				+				+	+					
Petaurista sp.			+													
Panthera cf. *tigris*			+													
P. pardus			+													
Pseudaxis grayi			+		+											
Pliohyaena licenti						+										
Palaeoloxodon namadicus						+										
Postschizotherium chardini						+										

Table 2. (*Continued*)

Taxa	Faunas															
	LD	WC	GWL	YG	CJW	XSG	DD1	DD2	DD3	DD4	DD5	DD6	DD7	HY	HBG2	HBG1
Paracamelus gigas						+										
Paenelimnoecus chinensis										+						
Paralactaga andersoni									+	+						
Pliosiphneus sp.								+	+							
Pliosiphneus sp. 2								+								
Pseudomeriones complicidens								+	+							
Palaeotragus sp.															+	
Postschizotherium sp.																+
Quyania sp.											+					
Rhinopithecus lantianensis			+													
Rusa elegans				+												
Sericolagus brachypus	+															
Sinicuon cf. *dubius*	+															
Sivapanthera linxiaensis	+															
Sus lydekkeri		+	+		+	+										
Scaptochirus moschatus			+													
Sivapanthera pleistocaenicus			+													
Stegodon orientalis			+													
Sinomegaloceros konwanlinensis			+													
Sinomegaceros					+											
Spirocerus wongi						+										
S. peii						+										
Saidomys sp.										+	+					
Sinocricetus procressus							+	+		+	+					
Sinocricetus zdanskyi									+	+	+					
Sminthoides fraudator										+	+					
Sorex sp.								+				+	+			
Sinoryx sp.																+
Tapirus sinensis			+													
Trimylus sp.										+						
Trischizolagus sp.							+									
Ungaromys spp.							+	+			+					
Ursus sp.		+														
Ursus cf. *etruscus*			+			+										
Ursus kokeni				+												
Vulpes chikushanensis	+					+										
Viverra sp.																+
Yangia omegodon		+														
Youngia tingi		+				+										

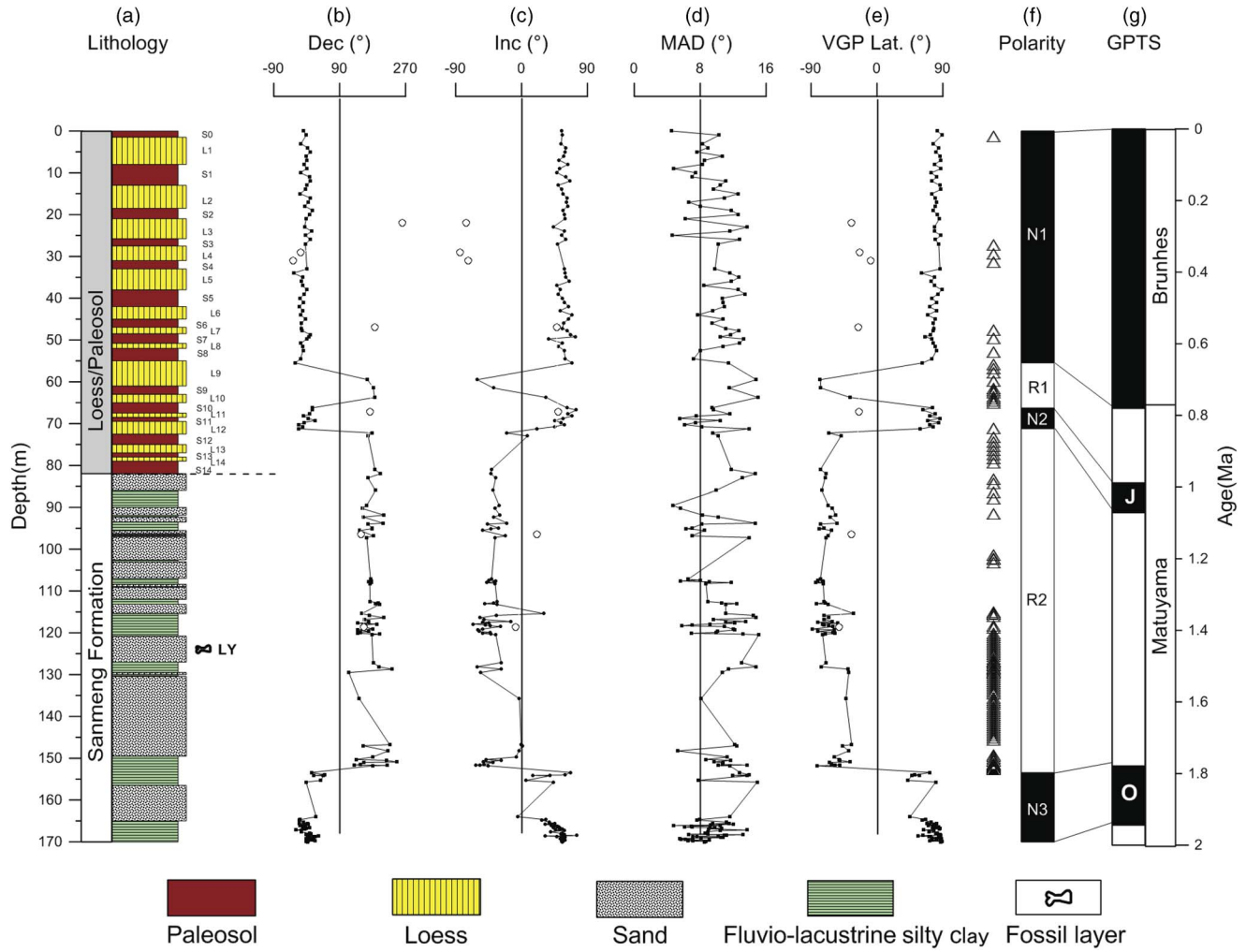

Figure 2. (color online) Magnetic polarity stratigraphy of the Linyi section. (a) Lithology. (b) Declination. (c) Inclination. (d) Maximum angular deviation (MAD). (e) Virtual geomagnetic pole (VGP) latitude. (f) Magnetic polarity sequence. (g) Geomagnetic polarity time scale (GPTS). Open circles represent rejected paleomagnetic data with inclinations <5° or paleomagnetic directions that are inconsistent with the expected geomagnetic field. Open triangles on the left-hand side of the polarity sequence represent rejected paleomagnetic data with unstable demagnetization trajectories at higher temperatures.

loess-paleosol sequence, and 198 block samples were taken at 10–25 cm intervals from the underlying silty clay and sand succession. From each block sample, cubic (2 cm × 2 cm × 2 cm) specimens were subsequently cut in the laboratory for stepwise thermal demagnetization analysis. In addition, 340 powdered samples were collected from the entire Linyi section for low-field magnetic susceptibility measurement (χ, calculated on a mass-specific basis), which is useful for establishing a time scale for the 82-m-thick loess-paleosol sequence.

The 340 powdered samples were packed into nonmagnetic cubic boxes (2 cm × 2 cm × 2 cm) for χ measurement with a Bartington Instruments MS2 magnetic susceptibility meter at 470 Hz. Temperature-dependent susceptibility ($\chi - T$) and isothermal remnant magnetization (IRM) acquisition measurements were conducted on six powdered samples selected from various lithologies and magnetic polarity zones of the Linyi section. All the χ–T curves were measured in an argon atmosphere at a frequency of 976 Hz from room temperature up to 700°C and back to room temperature using an MFK1-FA Kappabridge instrument equipped with a CS-3 high-temperature furnace. The magnetic field during measurement was 300 A/m (peak to peak). To determine the temperature-dependent background susceptibility, a run with an empty furnace tube was performed before measuring the sediment samples. The susceptibility of each sediment sample was obtained by subtracting the measured background susceptibility (furnace tube correction) using the CUREVAL 5.0 program (AGICO, Czech Republic). The IRM acquisition curves were determined using an ASC IM-10-30 pulse magnetizer (capable of generating fields up to a maximum field of 2 T) and an AGICO JR-6A spinner magnetometer for remanence measurements. A total of 31 IRM steps were performed.

Stepwise thermal demagnetization was conducted using a 2G Enterprises Model 755-R cryogenic magnetometer

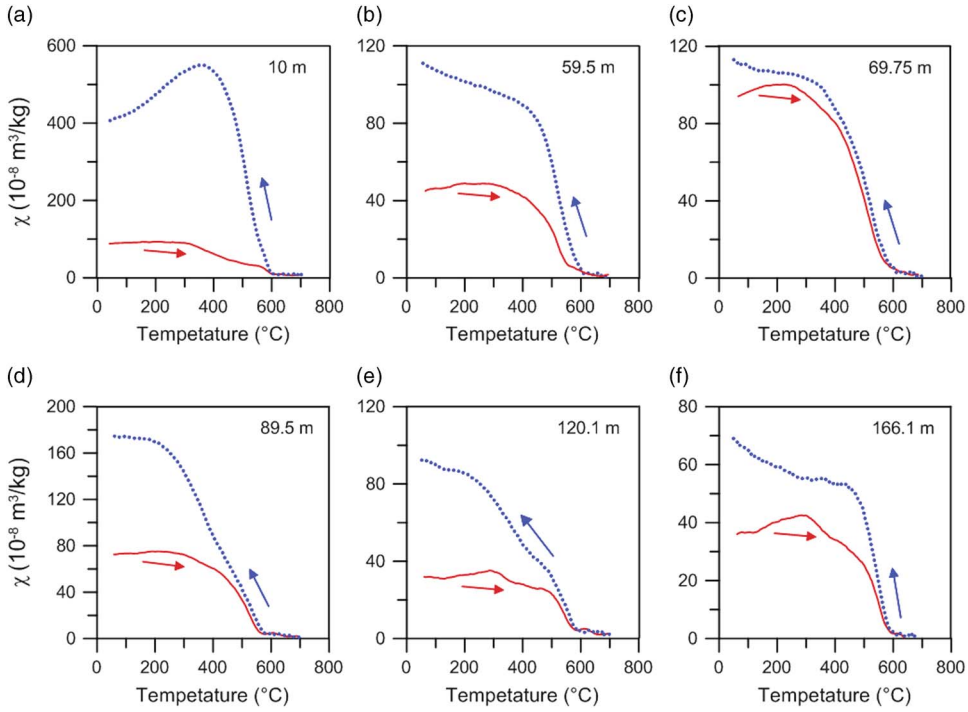

Figure 3. χ–T curves for six typical samples from the Linyi section. (a) 10 m (paleosol S1); (b) 59.5 m (loess L9); (c) 69.75 m (paleosol S11); (d) 89.5 m (silty clay); (e) 120.1 m (silty clay); (f) 166.1 m (silty clay). Red (blue) lines represent heating (cooling) curves. (For interpretation of the references to color in this figure legend, the reader is referred to the web version of this article.)

installed in a magnetically shielded laboratory (with ambient field <150 nT). All samples were stepwise heated in 14 steps at 25–50°C increments to a maximum temperature of 580°C. After each demagnetization step, the remanent magnetization of each sample was measured. Demagnetization results were evaluated using orthogonal vector component diagrams (Zijderveld, 1967), and the principal component direction was computed using least-squares fitting (Kirschvink, 1980). The principal component analyses were conducted using the PaleoMag software developed by Jones (2002).

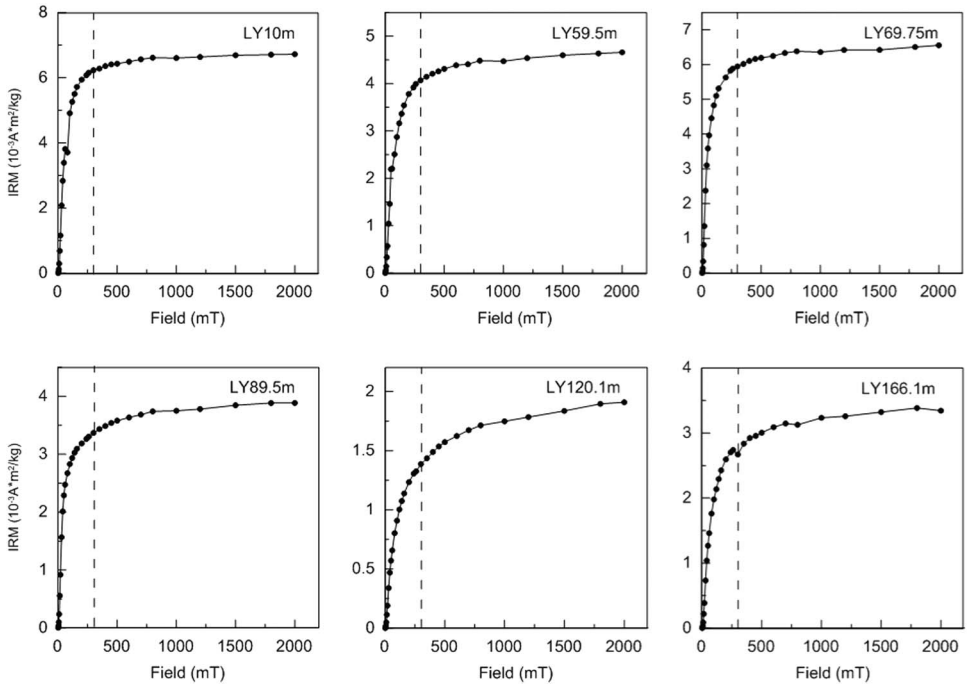

Figure 4. Isothermal remanent magnetization (IRM) acquisition curves for six typical samples from the Linyi section, the same levels as shown in Figure 3. The dashed vertical lines at 300 mT are shown to differentiate between low- and high-coercivity portions of the IRM acquisition curves.

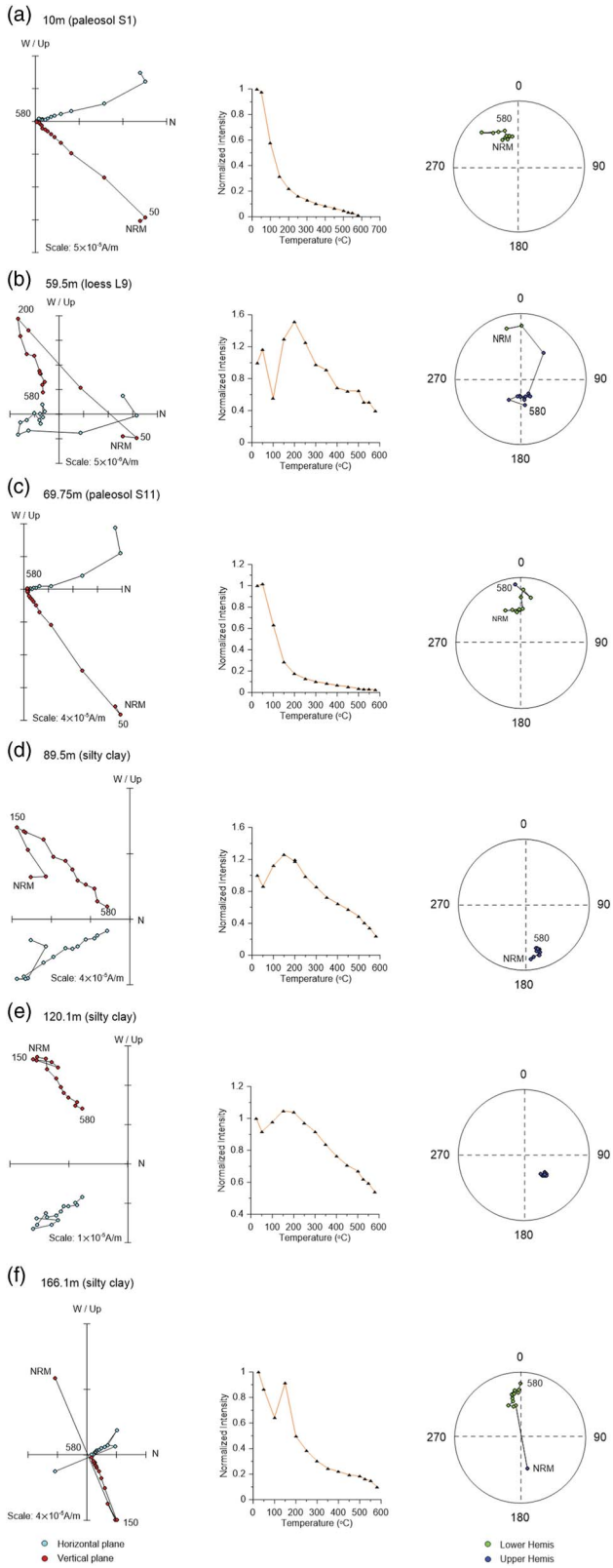

Figure 5. Demagnetization diagrams for stepwise thermal demagnetization of the natural remanent magnetization (NRM) data, their decay curves (plots in the second column), and corresponding equal-area stereographic projections (rightmost plots) for selected samples from the Linyi section (the same samples as in Figs. 3 and 4). (a) 10 m (paleosol S1); (b) 59.5 m (loess L9); (c) 69.75 m (paleosol S11); (d) 89.5 m (silty clay); (e) 120.1 m (silty clay); (f) 166.1 m (silty clay). Green and red circles in the orthogonal projections represent horizontal and vertical planes, respectively. Green and blue circles in the equal-area stereographic projections are mean lower hemis and upper hemis. The numbers refer to the temperatures in degrees Celsius. (For interpretation of the references to color in this figure legend, the reader is referred to the web version of this article.)

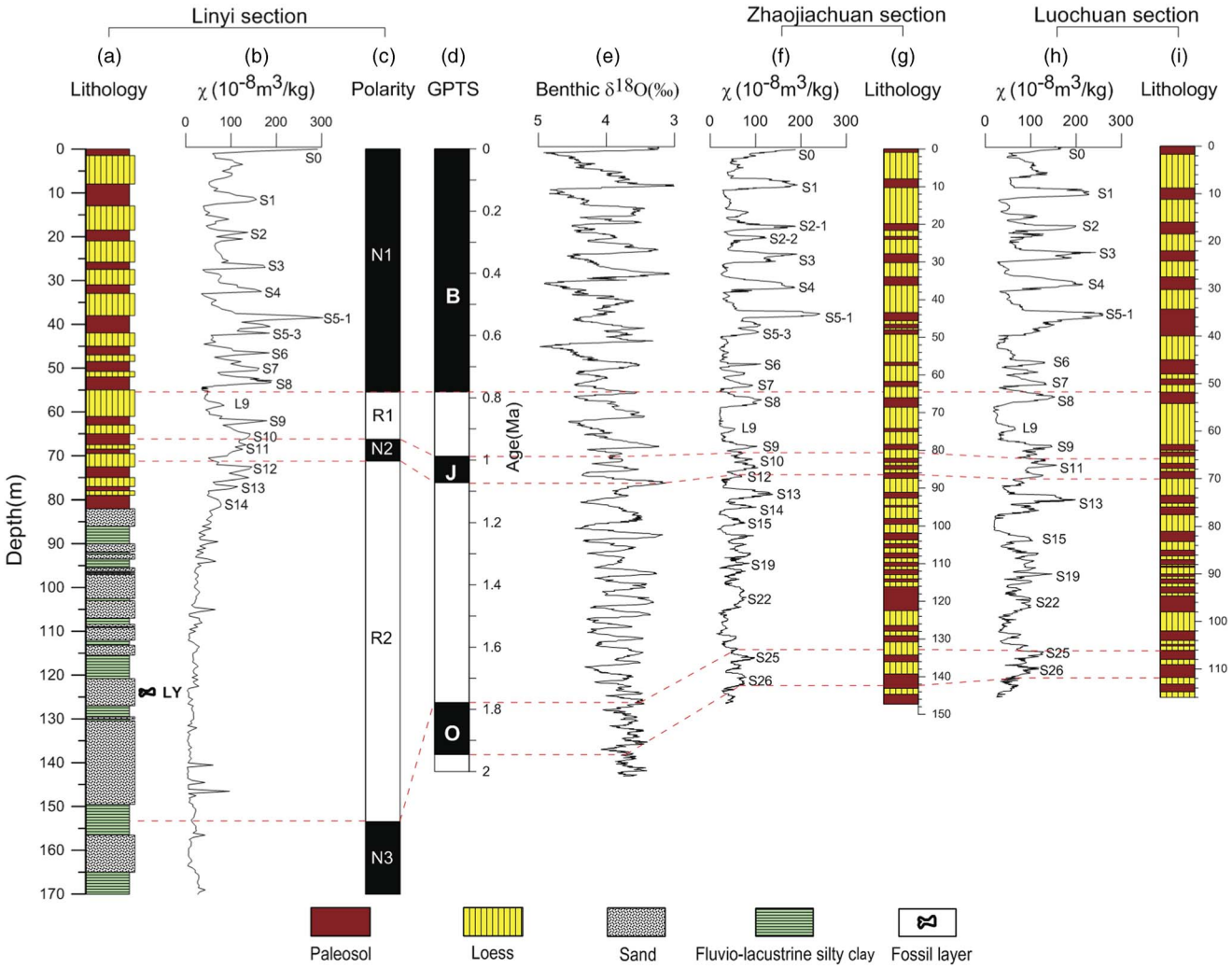

Figure 6. (color online) Lithostratigraphy, magnetic susceptibility stratigraphy, and magnetostratigraphy for the Linyi, Zhaojiachuan (Sun et al., 2006), and Luochuan (Liu, 1985; Lu et al., 1999) sections and correlations to the geomagnetic polarity time scale (GPTS) (Hilgen et al., 2012) and benthic δ^{18} O (‰) (Zachos et al., 2001). (a) Lithology of Linyi section. (b) Magnetic susceptibility of Linyi section. (c) Magnetic polarity sequence of Linyi section. (d) Geomagnetic polarity time scale (GPTS). (e) Benthic δ^{18} O (‰). (f) Magnetic susceptibility of Zhaojiachuan section. (g) Lithology of Zhaojiachuan section. (h) Magnetic susceptibility of Luochuan section. (i) Lithology of Luochuan section.

RESULTS

Magnetic properties

Consistent with the ubiquitous occurrence of magnetite, all the heating curves are characterized by an inflection at ~585°C (Fig. 3). A steady χ increase from room temperature to ~300°C is possibly attributable to gradual unblocking of fine-grained ferrimagnetic particles or the release of stress upon heating (Van Velzen and Zijderveld, 1995; Deng et al., 2004, 2006; Liu et al., 2005, 2010). A χ decrease at 300–500°C is generally interpreted as conversion of ferrimagnetic maghemite to weakly magnetic hematite (Florindo et al., 1999; Zhu et al., 2001; Deng et al., 2004, 2006) or changes in crystallinity, grain size, or morphology of the magnetic particles during heating (Dunlop and Özdemir, 1997; Ao, 2008; Ao et al., 2009, 2010). The cooling curves for six samples have much higher values than the corresponding heating curves, which indicates transformation of iron-containing clays or silicates to new ferrimagnetic minerals during heating (Hunt et al., 1995; Florindo et al., 1999; Zhu et al., 2001; Ao et al., 2009).

Consistent with the dominant contribution of magnetite to the magnetic mineralogy, all IRM acquisition curves undergo a major increase below 300 mT (Fig. 4). The additional slight increase in IRM after application of fields of >300 mT indicates the presence of high-coercivity hematite (Fig. 4).

Magneto-cyclostratigraphy

In most samples from the Linyi section, the natural remanent magnetization is composed of two components: (1) a secondary low-temperature component (LTC) isolated by progressive demagnetization to 150–250°C (occasionally up

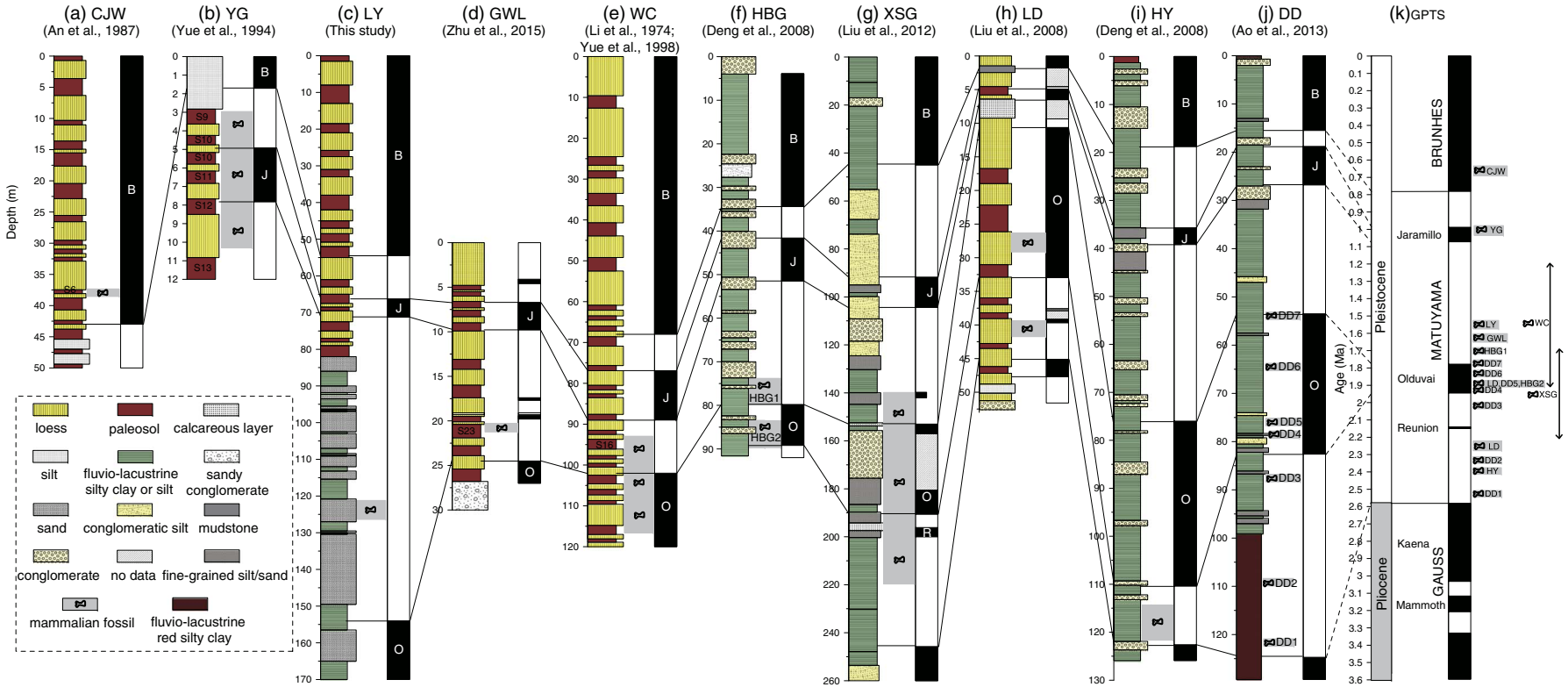

Figure 7. (color online) A synthetic diagram relating the magnetostratigraphically dated sections on the Chinese Loess Plateau, which contain the mammalian fauna sites, to the geomagnetic polarity time scale (GPTS). CJW, Chenjiawo; DD, Daodi; GWL, Gongwangling; HBG, Huabaogou; HY, Hongya; LD, Longdan; LY, Linyi; WC, Wucheng; XSG, Xiashagou; YG, Yangguo. (a) Lithology, Depth of fauna and Magnetic polarity sequence of CJW section. (b) Lithology, Depth of fauna and Magnetic polarity sequence of YG section. (c) Lithology, Depth of fauna and Magnetic polarity sequence of LY section. (d) Lithology, Depth of fauna and Magnetic polarity sequence of GWL section. (e) Lithology, Depth of fauna and Magnetic polarity sequence of WC section. (f) Lithology, Depth of fauna and Magnetic polarity sequence of HBG section. (g) Lithology, Depth of fauna and Magnetic polarity sequence of XSG section. (h) Lithology, Depth of fauna and Magnetic polarity sequence of LD section. (i) Lithology, Depth of fauna and Magnetic polarity sequence of HY section. (j) Lithology, Depth of fauna and Magnetic polarity sequence of DD section. (k) Geomagnetic polarity time scale (GPTS).

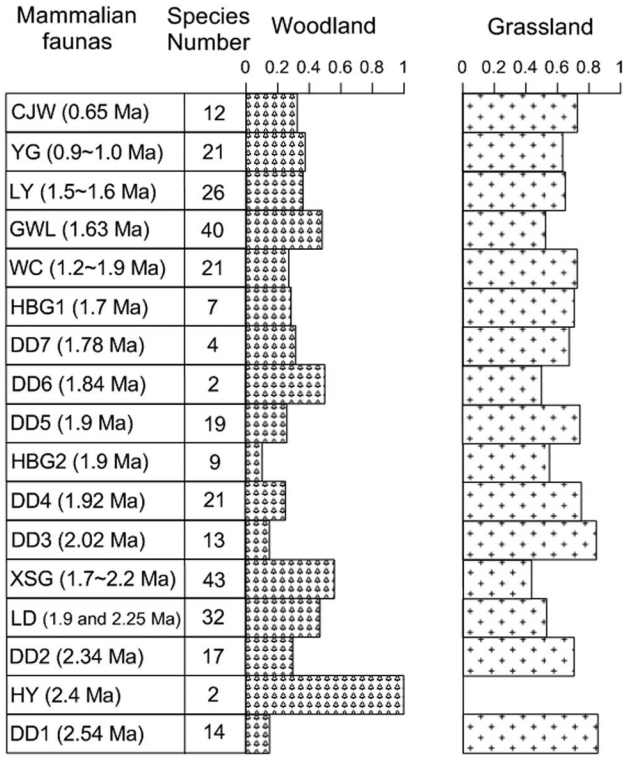

Figure 8. Variability of the total number of mammalian species and percentages of grassland and woodland groups for the well-dated Pleistocene faunas on the Chinese Loess Plateau. CJW, Chenjiawo; DD, Daodi; GWL, Gongwangling; HBG, Huabaogou; HY, Hongya; LD, Longdan; LY, Linyi; WC, Wucheng; XSG, Xiashagou; YG, Yangguo.

to 400°C) followed by (2) a characteristic remnant magnetization (ChRM) component isolated at higher temperatures (Fig. 5). The ChRM shows a relatively straightforward unidirectional trajectory toward the origin of orthogonal plots, while the LTC does not decay toward the origin for most samples. From the 296 demagnetized samples, there were 172 yield-stable ChRM components based on strict criteria: (1) data from at least four consecutive demagnetization steps were used for linear fitting, starting at least at 250°C; (2) a maximum angular deviation (MAD) <15° was required for the line fit; and (3) a calculated virtual geomagnetic pole (VGP) latitude >30° or <–30° (May and Butler, 1986; Zhu et al., 2007; Ao et al., 2013). The remaining 124 samples were excluded because they have unstable demagnetization trajectories, MAD values ≥15, VGP latitudes between –30° and 30°, or declinations trending roughly north (or south) but with upward (or downward) inclinations inconsistent with the expected field. Excluded samples tend to be associated with the fluvial-lacustrine interval that has a coarse-grained lithology of sand and silty clay (Fig. 2a). This might provide an explanation for the rather high proportion of excluded samples (42% of the total sample population). VGP latitudes calculated from all the 172 reliable ChRM directions are used to establish the magnetostratigraphic zonation, which allows identification of three normal and two reversed polarity zones (Fig. 2). Each polarity zone is defined based on at least two consecutive VGP latitudes of identical polarity. Correlation of the Linyi magnetic polarity sequence to the geomagnetic polarity time scale (Hilgen et al., 2012) suggests that the Linyi section records the Brunhes chron, Jaramillo and Olduvai subchrons, and successive reverse polarity portions of the intervening Matuyama chron (Figs. 2 and 6).

Consistent with the lithological transition from fluvial-lacustrine silty clay and sand sequence to the overlying eolian loess-paleosol sequence, the χ is shifted from low to high values (Fig. 6a and b). The χ for the fluvial-lacustrine silty clay and sand sequence (82–170 m) ranges from ~3×10^{-8} m^3/kg to ~100×10^{-8} m^3/kg, with an average of ~30×10^{-8} m^3/kg. The χ for the overlying loess-paleosol sequence (0–82 m) ranges from ~30×10^{-8} m^3/kg in loess to ~300×10^{-8} m^3/kg in some paleosols; such values are typical of Pleistocene loess-paleosol sequences from the CLP (Wang et al., 2005; Liu et al., 2015). Loess and paleosol layers are characterized by low and high χ, respectively. Temporal loess-paleosol χ variability of the Linyi section is closely correlated with that of other sections across the CLP, such as those at nearby Zhaojiachuan (Sun et al., 2006) and Luochuan (Liu, 1985; Lu et al., 1999) sections (Fig. 6). In particular, the composite paleosol S_5 with unusually high χ and redder color and loess L_9 with extremely coarse grain sizes, which are important marker layers in the Chinese loess-paleosol sequence (Liu, 1985), are clearly identified in the mid-Brunhes and prior to the Matuyama-Brunhes boundary in the Linyi section, respectively (Fig. 6). Based on this correlation, we found that the 82-m-thick Linyi loess-paleosol sequence ranges continuously from paleosol S_0 to S_{14}. The top paleosol is S_0, which formed during the present interglacial period (Sun et al., 2006).

DISCUSSION

The lithological and χ cycles of loess-paleosol sequences can be correlated from section to section across the CLP as well as cycle by cycle to benthic $\delta^{18}O$ records (Kukla et al., 1988; An et al., 1991; Heslop et al., 2000; Ding et al., 2002; Sun et al., 2006). At the Linyi section, the lithological and χ records indicate that the 82-m-thick loess-paleosol sequence continuously spans from paleosol layers S_0 to S_{14} (Fig. 6), covering the past 1.26 Ma (Sun et al., 2006). Brunhes chron, Jaramillo and Olduvai subchrons, and successive reverse polarity portions of the intervening Matuyama chron are successfully identified in the Linyi section (Fig. 6). The Brunhes-Matuyama boundary is identified in S_8 in the Linyi section, while the Jaramillo polarity subchron is identified in S_{10}–L_{12}. The termination of the Olduvai polarity subchron is identified at a depth of 153.4 m in the underlying fluvial-lacustrine sequence.

There are two potential age estimates for the Linyi Fauna. The first option yields an age of ~1.52–1.55 Ma for the Linyi Fauna, which is obtained via linear interpolation between Olduvai and Jaramillo polarity subchrons, assuming a constant long-term sedimentation rate between them. The eolian loess-paleosol sequence (71.25–82 m) prior to the Jaramillo polarity

subchron should have a lower sedimentation rate than the underlying fluvial-lacustrine silty clay and sand sequence (82–153.4 m) above the Olduvai polarity subchron. Assuming a constant sedimentation rate for the overlying eolian Quaternary yellowish loess-paleosol sequence and the underlying fluvial-lacustrine silty clay and sand sequence may have caused this age estimate to be slightly younger. The second yields an age of ~1.56–1.58 Ma, which is established by linear interpolation using the bottom age of paleosol S_{14} (Sun et al., 2006) and the top age of the Olduvai subchron (Hilgen et al., 2012) as constraints. The bottom of paleosol S_{14} has an age of 1.26 Ma as suggested by tuning the grain-size record to orbital obliquity and precession parameters (Sun et al., 2006). Considering the possible presence of unobservable small hiatuses and variations in sedimentation rate for the sand and silty clay deposits in the fluviolacustrine sequence, we suggest an age of 1.5–1.6 Ma for the Linyi Fauna.

Combining our new and previous paleomagnetic dating of faunas, we can now establish a magnetochronological framework for the faunas on the CLP. The previously published magnetostratigraphic data (Li et al., 1974; An et al., 1987; Yue et al., 1994; Deng et al., 2008; Liu et al., 2008, 2012; Ao et al., 2013) have suggested that the faunas of DD, HY, LD, XSG, HBG2, HBG1, WC, GWL, LY, and YG reside in the Matuyama chron, with only CJW in the Brunhes (Fig. 7; see figure caption for definition of abbreviations). More precisely, the DD Fauna appears to be located between the Gauss-Matuyama boundary and the termination of the Olduvai polarity subchron, ranging in age from ca. 2.5 to 1.8 Ma (Ao et al., 2013); LD Fauna has two mammal fossil layers, which occur during the early the Olduvai subchron and pre-Olduvai Matuyama chron, yielding an age between 2.25 and 1.9 Ma (Liu et al., 2008) (Fig. 7). The HY Fauna is located within the earliest Matuyama chron, with an age of 2.4 Ma. The XSG Fauna is located between the pre-Reunion Matuyama chron and the post-Olduvai Matuyama chron, with an age of 1.7–2.2 Ma. The HBG2 Fauna is located within the lower Olduvai polarity subchron, with an estimated age of ca 1.9 Ma, while the HBG1 Fauna occurs later than the termination of the Olduvai polarity subchron, with an estimated age of ca 1.7 Ma (Deng et al., 2008). The WC Fauna is located within the middle Matuyama chron, with an estimated age of ca. 1.2–1.9 Ma (Li et al., 1974; Yue et al., 1994, 1998). The GWL Fauna occurs during S_{22} or S_{23} of the Chinese loess-paleosol sequence, with an age of 1.54–1.65 Ma (Zhu et al., 2015). The CJW Fauna corresponds to S_6 based on the biochronology and stratigraphic correlation with typical loess-paleosol sequences of Luochuan, yielding an age of ~0.65 Ma (An et al., 1987; An and Kun, 1989) (Fig. 7). The YG Fauna occurs around the Jaramillo subchron, with an age of 0.98–1.05 Ma (Yue et al., 1994). Therefore, our established magnetochronological framework indicates that the CLP faunas range from ca 2.5 to 0.6 Ma, spanning most of the Pleistocene, with significantly flourishing faunas during the Early and Middle Pleistocene (Fig. 7).

The abundant faunas on the CLP contain both typical grassland and woodland species (Tables 1 and 2 indicate that mixed grassland and woodland habitats were prevalent during the Pleistocene). For these well-dated faunas, we further calculated the occurrence of woodland and grassland mammalian groups as percentages (Fig. 8). Overall, grassland mammals have higher percentages than woodland mammals in these faunas, which is consistent with the semiarid CLP environment during the Pleistocene (Liu, 1985; Maher, 2016), under the influence of global glacial-interglacial cycles (Figs. 2 and 6).

CONCLUSIONS

An integrated stratigraphic analysis, involving lithostratigraphy, magnetic susceptibility stratigraphy, and magnetostratigraphy, indicates that the Linyi section records a polarity pattern from the Brunhes chron to the Olduvai subchron. The Linyi Fauna's layer occurs in a reversed polarity magnetozone between the Olduvai and Jaramillo subchrons, yielding an estimated age of ~1.5–1.6 Ma. Combining our new and previous magnetostratigraphic dating of faunas, we establish a Pleistocene magnetochronology spanning from 2.54 to 0.65 Ma for the faunas on the CLP.

ACKNOWLEDGMENTS

We are grateful to Randall Schaetzl for his suggestions that improved the paper and PhD student Yang Yi from the Nanjing Institute of Geology and Palaeontology, Chinese Academy of Sciences for help in sampling and experiments. Thank you for the comments provided by the editors and two reviewers. This work was supported financially by the National Natural Science Foundation of China (grant 41372020) and the Key Research Program of Frontier Sciences, Chinese Academy of Sciences (grants QYZDB-SSW-DQC021, QYZDY-SSW-DQC001, and ZDBS-SSW-DQC001).

REFERENCES

An, Z.S., Kukla, G., Porter, S.C., Xiao, J.L., 1991. Late quaternary dust flow on the Chinese Loess Plateau. *Catena* 18, 125–132.

An, Z.S., Kun, H.C., 1989. New magnetostratigraphic dates of Lantian *Homo erectus*. *Acta Anthropologica Sinica* 32, 213–221.

An, Z.S., Liu, T.S., Kan, X.F., Sun, J.Z., Wang, J.D., Kao, W.Y., Zhu, Y.Z., Wei, M.J., 1987. Loess-paleosol sequences and chronology at Lantian Man localities. In: Liu, T.S. (Ed.), Aspects of Loess Research. China Ocean Press, Beijing, pp. 192–203.

Ao, H., 2008. Rock magnetic properties of the fluvio-lacustrine sediments from the Dachangliang section in the Nihewan Basin, northern China. [In Chinese with English abstract.] *Chinese Journal of Geophysics* 51, 1029–1039.

Ao, H., An, Z.S., Dekkers, M.J., Li, Y., Xiao, G.Q., Zhao, H., Qiang, X.K., 2013. Pleistocene magnetochronology of the fauna and Paleolithic sites in the Nihewan Basin: significance for environmental and hominin evolution in North China. *Quaternary Geochronology* 18, 78–92.

Ao, H., Dekkers, M.J., Deng, C.L., Zhu, R.X., 2009. Paleoclimatic significance of the Xiantai fluvio-lacustrine sequence in the Nihewan Basin (North China), based on rock magnetic properties

and clay mineralogy. *Geophysical Journal International* 177, 913–924.

Ao, H., Deng, C.L., Dekkers, M.J., Sun, Y., Liu, Q., Zhu, R.X., 2010. Pleistocene environmental evolution in the Nihewan Basin and implication for early human colonization of North China. *Quaternary International* 223, 472–478.

Ao, H., Roberts, A.P., Dekkers, M.J., Liu, X.D., Rohling, E.J., Shi, Z.G., An, Z.S., Zhao, X., 2016. Late Miocene–Pliocene Asian monsoon intensification linked to Antarctic ice-sheet growth. *Earth and Planetary Science Letters* 444, 75–87.

Cai, B.Q., 1987. A preliminary report on the late Pliocene micromammalian fauna from Yangyuan and Yuxian, Hebei. [In Chinese with English abstract.] *Vertebrata Palasiatica* 25, 124–136.

Cai, B.Q., Zhang, Z.Q., Zheng, S.H., Qiu, Z.D., Li, Q., 2004. New advances in the stratigraphic study on representative sections in the Nihewan Basin. [In Chinese with English abstract.] *Heibei. Professional Papers on Stratigraphy and Paleontology* 28, 267–285.

Deng, C.L., Shaw, J., Liu, Q.S., Pan, Y.X., Zhu, R.X., 2006. Mineral magnetic variation of the Jingbian loess/paleosol sequence in the northern Loess Plateau of China: implications for Quaternary development of Asian aridification and cooling. *Earth and Planetary Science Letters* 241, 248–259.

Deng, C.L., Zhu, R.X., Verosub, K.L., Singer, M.J., Vidic, N.J., 2004. Mineral magnetic properties of loess/paleosol couplets of the central loess plateau of China over the last 1.2 Myr. Journal of Geophysical Research 109, B01103. http://dx.doi.org/10.1029/2003JB002532.

Deng, C.L., Zhu, R.X., Zhang, R., Ao, H., Pan, Y.X., 2008. Timing of the Nihewan formation and faunas. *Quaternary Research* 69, 77–90.

Ding, Z.L., Derbyshire, E., Yang, S., Yu, Z., Xiong, S., Liu, T., 2002. Stacked 2.6-Ma grain size record from the Chinese loess based on five sections and correlation with the deep-sea $\delta^{18}O$ record. *Paleoceanography* 17, 5–1–5-21.

Ding, Z.L., Liu, T.S., Rutter, N.W., Yu, Z.W., Guo, Z.T., 1995. Ice-volume forcing of East Asian winter monsoon variations in the past 800,000 years. *Quaternary Research* 44, 149–159.

Dunlop, D.J., Özdemir, Ö., 1997. Rock Magnetism: Fundamentals and Frontiers. Cambridge University Press, Cambridge.

Florindo, F., Zhu, R., Guo, B., Yue, L., Pan, Y., Speranza, F., 1999. Magnetic proxy climate results from the Duanjiapo loess section, southernmost extremity of the Chinese loess plateau. *Journal of Geophysical Research* 104, 645–659.

Heslop, D., Langereis, C.G., Dekkers, M.J., 2000. A new astronomical timescale for the loess deposits of northern China. *Earth and Planetary Science Letters* 184, 125–139.

Hilgen, F.J., Lourens, L.J., van Dam, J.A., 2012. The Neogene period. In: Gradstein, F.M., Ogg, J.G., Schmitz, M., Ogg, G. (Eds.), *The Geologic Time Scale*. Elsevier, Amsterdam, pp. 923–978.

Huang, W.P., Tang, Y.J., 1974. Observation on the later Cenozoic of Nihewan Basin. [In Chinese with English abstract.] *Vertebrata Palasiatica* 12, 99–110.

Hunt, C.P., Banerjee, S.K., Han, J., Solheid, P.A., Oches, E., Sun, W., Liu, T., 1995. Rock-magnetic proxies of climate change in the loess-paleosol sequences of the western Loess Plateau of China. *Geophysical Journal International* 123, 232–244.

Jones, C.H., 2002. User-driven integrated software lives: "PaleoMag" paleomagnetics analysis on the Macintosh. *Computers & Geosciences* 28, 1145–1151.

Kirschvink, J.L., 1980. The least-squares line and plane and the analysis of palaeomagnetic data. *Geophysical Journal International* 62, 699–718.

Kukla, G., Heller, F., Liu, X., Xu, T., Liu, T., An, Z.S., 1988. Pleistocene climates in China dated by magnetic susceptibility. *Geology* 16, 811–814.

Li, H.M., An, Z.S., Wang, J.D., 1974. Preliminary paleomagnetic study of loess form the Wucheng section, northern China. *Geochimica* 6, 93–104.

Li, X.W., Ao, H., Dekkers, M.J., Roberts, A.P., Zhang, P., Lin, S., Huang, W.W., Hou, Y.M., Zhang, W.H., An, Z.S., 2017. Early Pleistocene occurrence of Acheulian technology in North China. *Quaternary Science Reviews* 156, 12–22.

Li, Q., Zheng, S.H., Cai, B.Q., 2008. Pliocene biostratigraphic sequence in the Nihewan Basin, Hebei, China. [In Chinese with English abstract.] *Vertebrata Palasiatica* 46, 210e232.

Liu, P., Deng, C.L., Li, S.H., Cai, S.H., Cheng, H.J., Yuan, B.Y., Wei, Q., Zhu, R.X., 2012. Magnetostratigraphic dating of the Xiashagou Fauna and implication for sequencing the mammalian faunas in the Nihewan Basin, North China. *Palaeogeography, Palaeoclimatology, Palaeoecology* 315–316, 75–85.

Liu, P., Deng, C.L., Li, S.H., Zhu, R.X., 2010. Magnetostratigraphic dating of the Huojiadi Paleolithic site in the Nihewan Basin, North China. *Palaeogeography, Palaeoclimatology, Palaeoecology* 298, 399–408.

Liu, P., Zhang, S., Han, J.M, Liu, T.S., 2008. Paleomagnetic chronology of Quaternary stratigraphy of the Longdan section in Gansu province of China. [In Chinese with English abstract.] *Quaternary Sciences* 28, 796–805.

Liu, Q., Deng, C., Yu, Y., Torrent, J., Jackson, M.J., Banerjee, S.K., Zhu, R.X., 2005. Temperature dependence of magnetic susceptibility in argon environment: implications for pedogenesis of Chinese loess/palaeosols. *Geophysical Journal International* 161, 102–112.

Liu, Q., Jin, C., Hu, P., Jiang, Z., Ge, K., Roberts, A.P., 2015. Magnetostratigraphy of Chinese loess–paleosol sequences. *Earth-Science Reviews* 150, 139–167.

Liu, T.S., 1985. Loess and Environment. Science Press, Beijing.

Lu, H.Y., Liu, X.D., Zhang, F.Q., An, Z.S., Dodson, J., 1999. Astronomical calibration of loess–paleosol deposits at Luochuan, central Chinese Loess Plateau. *Palaeogeography, Palaeoclimatology, Palaeoecology* 154, 237–246.

Maher, B.A., 2016. Palaeoclimatic records of the loess/palaeosol sequences of the Chinese Loess Plateau. *Quaternary Science Reviews* 154, 23–84.

May, S.R., Butler, R.F., 1986. North American Jurassic apparent polar wander: implications for plate motion, paleogeography and Cordilleran tectonics. *Journal of Geophysical Research* 91, 11519–11544.

Porter, S.C., An, Z.S., 1995. Correlation between climate events in the North Atlantic and China during the last Glaciation. *Nature* 375, 305–308.

Qiu, Z.X., Qiu, Z.D., 1995. Chronological sequence and subdivision of chinese neogene mammalian faunas. *Palaeogeography Palaeoclimatology Palaeoecology* 116(1-2), 41–70.

Sun, Y., Clemens, S.C., An, Z., Yu, Z., 2006. Astronomical timescale and palaeoclimatic implication of stacked 3.6-Myr monsoon records from the Chinese Loess Plateau. *Quaternary Science Reviews* 25, 33–48.

Tang, Y.J., Zong, G.F., Xu, Q.Q., 1983. Mammalian fossils and stratigraphy of Linyi, Shanxi. [In Chinese with English abstract.] *Vertebrata Palasiatica* 21, 77–86.

Tong, H.W., Li, H., Xie, J.Y., 2008. Revisions of some taxa of the Salawusu fauna from Sjara-Osso-Gol area, Neimongol, China. [In Chinese with English abstract.] *Quaternary Sciences* 28, 1106–1113.

Van Velzen, A.J., Zijderveld, J.D.A., 1995. Effects of weathering on single-domain magnetite in Early Pliocene marine marls. *Geophysical Journal International* 121, 267–278.

Wang, A.D., 1982. Discovery of the Pliocene mammalian faunas from the Nihewan region and its significance. *Chinese Science Bulletin* 27, 227–229.

Wang, X., Løvlie, R., Yang, Z., Pei, J., Zhao, Z., Sun, Z., 2005. Remagnetization of Quaternary eolian deposits: a case study from SE Chinese Loess Plateau. *Geochemistry, Geophysics, Geosystems* 6, Q06H18. http://dx.doi.org/10.1029/2004GC000901.

Wen, Q.Z., 1989. Chinese Loess Geochemistry. Science Press, Beijing.

Xiao, J.L., Porter, S.C., An, Z.S., Kumai, H., Yoshikawa, S., 1995. Grain size of quartz as an indicator of winter monsoon strength on the Loess Plateau of central China during the last 130,000 yr. [In Chinese with English abstract.] *Quaternary Research* 43, 22–29.

Xue, X.X., Zhang, Y.X., Yue, L.P., 2006. The environment and climate evolution of loess and red clay series on Chinese Loess Plateau through the mammalian fossils. [In Chinese with English abstract.] *Science in china series D: Earth Sciences* 36, 359–369.

Yue, L.P., Wang, Y., Zheng, H.B., 1994. Magnetostratigraphic date on the "Yangguo Fauna.". [In Chinese with English abstract.] *Journal of Stratigraphy* 18, 203–206.

Yue, L.P., Xue, X.X., 1996. The comparative study of magnetostratigraphy and biostratigraphy in Chinese loess area. [In Chinese with English abstract.] *Quaternary Sciences* 3, 239–245.

Yue, L.P., Zhang, Y.X., Deng, X.Q., Zhang, L., 1998. Mammalian faunas and magnetostratigraphic sequence in North China since 5.30Ma. [In Chinese with English abstract.] *Journal of Stratigraphy* 22, 206–210.

Zachos, J., Pagani, M., Sloan, L., Thomas, E., Billups, K., 2001. Trends, rhythms, and aberrations in global climate 65 Ma to present. *Science* 292, 686–693.

Zhang, Z.Q., Zheng, S.H., Liu, J.B., 2003. Pliocene micromammalian biostratigraphy of Nihewan Basin, with comments on the stratigraphic division. [In Chinese with English abstract.] *Vertebrata Palasiatica* 41, 306–313.

Zhou, T.R., Li, H.Z., Liu, Q.S., Li, R.Q., Sun, X.P. 1991. *Cenozoic Paleogeography of the Nihewan Basin*. China Science Press, Beijing.

Zhou, M.Z., Zhou, B.X., 1959. Villafranchian mammals from Lingyi, S.W. Shansi. [In Chinese with English abstract.] *Acta Palaeontologica Sinica* 7, 89–97.

Zhou, M.Z., Zhou, B.X., 1965. Notes on Villafranchian mammals of Lingyi, Shanxi. [In Chinese with English abstract.] *Acta Palaeontologica Sinica* 9, 223–230.

Zhu, R.X., Deng, C.L., Jackson, M.J., 2001. A magnetic investigation along a NW-SE transect of the Chinese Loess Plateau and its implications. *Physics and Chemistry of the Earth* 26, 867–872.

Zhu, R.X., Deng, C.L., Pan, Y.X., 2007. Magnetochronology of the fluvio-lacustrine sequences in the Nihewan Basin and its implications for early human colonization of northeast Asia. *Quaternary Sciences* 27, 78–82 (in Chinese with English abstract).

Zhu, Z.Y., Dennell, R., Huang, W.-W., Wu, Y., Rao, Z.-G., Qiu, S.-F., Xie, J.-B., *et al*. 2015. New dating of the *Homo erectus* cranium from Lantian (Gongwangling), China. *Journal of Human Evolution* 78, 144–157.

Zijderveld, J.D.A., 1967. A.C. demagnetization of rocks: analysis of results. In: Collinson, D.W., Creer, K.M., Runcorn, S.K. (Eds.), Methods in Paleomagnetism. Elsevier, New York, pp. 254–286.